Rare Metal Materials and Engineering
Volume 50, Issue 11, November 2021
Available online at www.rmme.ac.cn

Science Press

Cite this article as: Wang Ziping, Fei Yue, Qian Lei, et al. Structural Optimization Design for Single Layer Surface Acoustic Wave Interdigital Transducer (SAW-IDT)[J]. Rare Metal Materials and Engineering, 2021, 50(11): 3917-3923.

ARTICLE

Structural Optimization Design for Single Layer Surface Acoustic Wave Interdigital Transducer (SAW-IDT)

Wang Ziping[1,2], Fei Yue[1], Qian Lei[1], Xue Xian[1], Karthik Reddy [2]

[1] National Center for International Research on Structural Health Management of Critical Components, Faculty of Civil Engineering and Mechanics, Jiangsu University, Zhenjiang 212013, China; [2] Department of Mechanical and Aerospace Engineering, North Carolina State University, Raleigh 27606, US

Abstract: In order to optimize the actuating performance of single layer surface acoustic wave interdigital transducer (SAW-IDT) and to improve the deficiencies of calculation process of the δ function analysis method, the static properties of the SAW-IDT were analyzed by the finite element simulation optimization method. The influence of the width of the branch electrodes (w), the electrodes interval (s), and the thickness of the substrate (t) on the actuating performance of SAW-IDT was investigated. The simulation results show that when w/t=0.7, the optimal strain response can be obtained; when s/t>3.2, the maximum strain can be obtained. Besides, it can also be concluded that the smaller the electrode interval, the lower the actuating voltage. According to the simulated optimization results, a SAW-IDT was prepared and the frequency response was tested by experiments. The results provide a guidance for the preparation, performance testing, and application of SAW-IDT.

Key words: interdigital transducer; structural optimization design; actuating performance

Surface acoustic wave (SAW) transducers generally use a combination of interdigital electrodes and piezoelectric material substrate, which combines the piezoelectric activity of piezoelectric ceramics with a certain flexibility and low acoustic impedance of polymers. SAW transducer has a high thickness electromechanical coupling coefficient, high piezoelectric strain constant, low mechanical quality factor, and low acoustic impedance[1]. It is suitable for producing transducers with high-sensitivity, wide-band, and narrow-pulse, and can be used in the fields of communication, structural health monitoring (SHM), and medical ultrasound[2-5].

The interdigital transducer (IDT) technology originates from the development of SAW devices. In recent years, it has gradually been used to guide wave detection based on SHM system[6-8]. Fig. 1 shows that the single layer IDTs have comb electrode characteristics. λ represents the width of a pair of interdigital electrodes and the cycle of the drive signal, and w means the width of a single electrode. The characteristics of the electrode can be placed on one side or both sides of the piezoelectric substrate. The frequency characteristics of the electrode correspond to the geometry of IDT fingers and have the function of modal selection[9-12]. Since IDT can form a directional actuating function through the arrangement of interdigitated electrodes, the low sidelobe directional waves can be generated based on this configuration without complicated electrode actuating. Jin et al[13] constructed IDTs to generate guided waves for non-destructive evaluation (NDE). The inspection capabilities of IDTs were verified to be superior to those of ordinary piezoelectric transducers. IDTs have been used in structures such as planes and surfaces. Monkhouse et al[14] constructed IDTs for exciting and receiving pipeline guided waves on polyvinylidene fluoride (PVDF) membrane substrates. The guided wave mode selection with phase velocity was used and the group velocity decay curves were tested. The actuating capability of the A_0 modal guided wave with an excitation frequency of 0.95 MHz was verified by the finite element methods. Hayward et al[15]

Received date: November 29, 2020
Foundation item: National Natural Science Foundation of China (11872191, 11520101001); Postgraduate Research & Practice Innovation Program of Jiangsu Province (KYCX20_3073)
Corresponding author: Wang Ziping, Ph. D, Associate Professor, Faculty of Civil Engineering and Mechanics, Jiangsu University, Zhenjiang 212013, P. R. China, E-mail: wzpxx2004@126.com

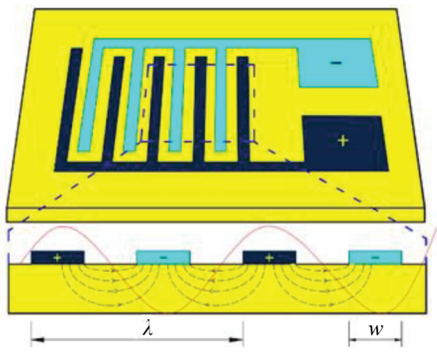

Fig.1 Schematic diagram of conventional single layer electrode IDT structure

placed the IDT on the piezoelectric composite layer between two polychlorinated biphenyls (PCBs) to realize wave number selection and modal selection. Based on the theory of wavelength-tunable actuators, Ren et al[16] proposed the concept of six circular arrays of PVDF curved IDTs, which allows each element to produce a diverging beam for examining the sectoral slice area of the plate. The detection range makes the operation point of guided wave test flexible. However, the directivity of IDTs depends on the number of finger electrodes, the frequency of excitation, and the piezoelectric constant d_{31} or d_{33} of the composite material. The most commonly used IDTs have been developed on both active fiber composite (AFC) and macro-fiber composite (MFC) structures in the form of equally spaced IDTs[17], weighted IDTs[18], slanted IDTs[19], annular focusing IDTs[20], and spiral MFC direction transducers[21]. IDTs with different design forms and different functions have always been an attractive topic in the current researches of guided wave excitation. The main optimization analysis methods of IDT include the δ function analysis method[22], extraction finger weighting method[23], equivalent circuit model method[24], and component object model (COM) theory[25]. Kuznetsova[26] presented an analytical solution for the Lamb waves stimulated by IDT to find a frequency range where the real part of velocity of evanescent wave is more than the imaginary one. In this region, the evanescent mode characterized by opposite directions of the phase and group velocities also indicates the backward wave.

According to requirements of SAW-IDT actuating performance, a theoretical simulation optimization analysis was conducted in this research. The influence of the width w of the branch electrodes, the interval s of the branch electrodes, and the thickness t of the substrate on the actuating performance was studied. Based on the relationship between the strain response and electrode width and between substrate thickness and electrode interval, an optimized design for improving the SAW-IDT actuating performance was obtained. This research provided a guideline for the preparation, performance testing, and application of SAW-IDT.

1 Single Layer IDT Working Principle

The device for excitation of SAW in solid material must be able to excite the particle displacement of the elastic surface wave. Assuming that u_1 and u_3 are two particle displacement components of Rayleigh SAW[27,28] and the phase difference is $\pi/2$, the excitation device must be able to generate the two-mass point displacement components u_1 and u_3 with the phase difference of $\pi/2$. For an IDT on a single crystal substrate, d_{11} is set as the piezoelectric coefficient of the single layer substrate due to its anisotropy and the piezoelectric equation. The relationship between the strain S of the excitation electric field (E_1, E_2, E_3) and the particle displacement u_i (i=1, 2, 3) in piezoelectric crystal can be expressed by a matrix, as follows:

$$\begin{bmatrix} S_{11} \\ S_{22} \\ S_{33} \\ S_{23} \\ S_{13} \\ S_{12} \end{bmatrix} = \begin{bmatrix} 0 & -d_{22} & d_{31} \\ 0 & d_{22} & d_{31} \\ 0 & 0 & d_{33} \\ 0 & d_{15} & 0 \\ d_{15} & 0 & 0 \\ -2d_{22} & 0 & 0 \end{bmatrix} \begin{bmatrix} E_1 \\ E_2 \\ E_3 \end{bmatrix} \tag{1}$$

where d_{22}, d_{15}, d_{31}, and d_{33} are the piezoelectric strain constants along different directions; E_1, E_2, and E_3 are the electric field components; S_{11}, S_{22}, S_{33}, S_{23}, S_{13}, and S_{12} are the components of the elastic strain S of the piezoelectric materials. According to Eq. (1), the applied electric field along x_1 direction can stimulate not only the particle displacement and strain along the x_1 direction, but also the strains along x_2 and x_3 directions. Fig. 2 shows the schematic diagram of the electric field excitation based on the assumption that IDT excites the wave propagating along x direction. Since IDT only excites the electric field along x_1 and x_3 directions in the substrate, the relationship between the particle displacement and strain components of the excited particle in Eq.(1) can be expressed as follows:

$$\begin{aligned} S_{11} &= \frac{\partial u_1}{\partial x_1} = d_{31} E_3 \\ S_{13} &= \frac{1}{2}\left(\frac{\partial u_1}{\partial x_3} + \frac{\partial u_3}{\partial x_1}\right) = d_{15} E_1 \end{aligned} \tag{2}$$

The phase difference between the IDT alternating electric fields E_1 and E_3 in Fig.2 is $\pi/2$. Therefore, the phase difference between u_1 and u_3 is also $\pi/2$. This characteristic of particle displacement component is exactly what Rayleigh SAW possesses. It is clear that IDT can stimulate Rayleigh SAW. According to the wave interference principle, when the frequency of the applied electric field signal of IDT is equal to the acoustic frequency corresponding to the period length of the interdigital electrode, the waves excited by each pair of interdigital electrodes are added at the same phase.

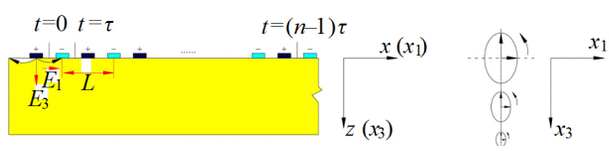

Fig.2 Schematic diagram of IDT excited electric field on piezoelectric transducer (PZT) substrate

Meanwhile, the IDT can stimulate the strongest SAW. If the frequency of the external electric field is different from that of the acoustic wave corresponding to the interdigital electrodes, the SAW excited by each pair of interdigital electrodes cannot be added at the same phase. So, the wave excited by the entire IDT will be weakened. The basic mechanism of Rayleigh SAW excited by IDT suggests that IDT can perform frequency selection. The optimal design of the IDT structure can excite the SAW with the strongest energy in different forms.

2 SAW-IDT Finite Element Modeling

The SAW-IDT deformation is divided into four stages[29]: (1) the piezoelectric substrate phase and the IDT polymer phase are linearly and elastically deformed; (2) the piezoelectric phase undergoes linear elastic deformation, and the polymer phase nonlinearly deforms; (3) the piezoelectric phase and the polymer phase are nonlinearly deformed; (4) IDT breaks as the piezoelectric material breaks.

Because IDT was used in elastic deformation area as a transducer, the deformation of the analysis process in this research could only possess the first deformation stage. The structural deformation of the SAW-IDT actuating element belongs to the small strain and small deformation, which conforms to Hooke's law. Software COMSOL was used to establish a mathematical model according to the following steps.

The selection of geometric parameters of the IDT electrode has an important influence on the ability of excitation of high-frequency acoustic waves and the concentration effect of the oil separation particles. In order to obtain the relationship between IDT inter-parameters, the optimization design was conducted. Fig. 3 shows the profile diagram of single layer IDT electrode profile, where w represents the electrode width, s represents the electrode interval, and t represents the substrate thickness. The structural features of electrode are indicated by the facts that positive and negative branch electrodes are arranged in an intersecting manner along the x-axis, and each branch electrode is connected by a pair of opposite main electrodes. The electrode structures on the upper and lower surfaces are completely symmetrical. The electric field is uniformly distributed only in a region far from the electrode and unevenly distributed near the electrode region. The area directly below the electrode is called the "dead zone" due to the low field strength, which is indicated by the dashed area in Fig.3.

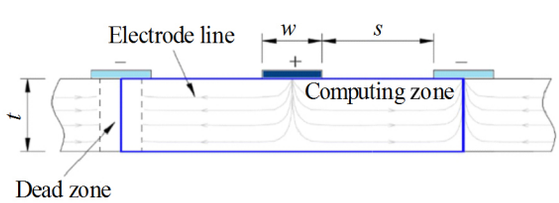

Fig.3 Schematic profile diagram of single layer IDT electrode

After the finite element model was established, some assumptions could be made: the polarization direction of the piezoelectric substrate is parallel to the x-axis; the polarization intensity of the piezoelectric substrate is uniformly distributed. To establish a simulation model on x-z plane and to construct the SAW element, it is essential to design the piezoelectric phase in the element's construction scheme, and to fully consider the influence of the volume ratio of the piezoelectric phase on the composite material, the elastic constant of the polymer material, and other electrical characteristics. The related piezoelectric substrate parameters used the actual PZT-51 parameters, as listed in Table 1. δ indicates the flexibility coefficient along different directions; ε_{11} and ε_{33} are the dielectrics constants along x and z directions, respectively; d_{31} and d_{33} are the piezoelectric strain constants along x and z directions, respectively; ρ and μ are the density and Poisson's ratio of piezoelectric material substrate, respectively. The parameters of electrode material were set according to those of DAD-40 type epoxy conductive adhesive (shear strength at room temperature of 14.7 MPa, volume resistivity≤1.0×10^{-3} Ω·cm). The electrode was configured as a strip-shaped cross electrode, and electrodes on both sides could generate opposite polarity electric fields. The boundary displacement constraint condition was: when X=0, 1, the model is free along x direction; when Y=0, the boundary is stable, i.e., when U_y=0 and Y=t, the upper surface of the model is free. An electric potential difference was applied on the electrodes on the upper surface by setting the negative electrode area as electrical ground and setting the positive electrode as 50 V. The finite element model and the related mesh are shown in Fig. 4. Meshing with four-node quadrangular elements was performed in the solid domain. The direct stationary solver was employed to calculate the steady state of the numerical model. The nonlinearity was automatically detected through analysis of the variables of the residual Jacobian matrix and the constraint Jacobian matrix. With a relative tolerance of 10^{-3}, all the calculations converge within 25 iterations. Here the piezoelectric device interface consisting of the electrostatic interface and the solid mechanic interface was used to conduct the stationary study.

3 SAW-IDT Structure Simulation Analysis

3.1 Effect of electrode width w on SAW-IDT performance

Fig.5a shows the influence of electrode width w or substrate thickness t on electric field. The strain length and the

Table 1 Material parameters of piezoceramic substrate (PZT-51)

Flexibility coefficient/ $\times10^{-12}$ m^2·N^{-1}			Dielectric constant		Piezoelectric strain constant/ $\times10^{-10}$ C·N^{-1}		Density, ρ/ g·cm^{-3}	Poisson's ratio, μ
δ_{11}^E	δ_{33}^E	S_{55}^E	ε_{11}	ε_{33}	d_{31}	d_{33}		
15.8	22.9	20.7	3400	3800	−2.75	6.8	7.45	0.32

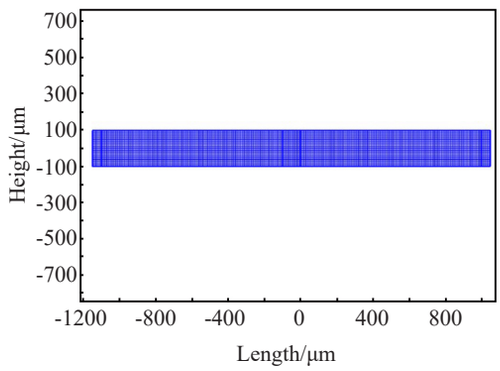

Fig.4 Finite element model and related mesh

thickness direction are alternately changed. The corresponding unit voltage is used when the ratio of the electrode width to the thickness of the piezoelectric substrate changes. The change trends of voltage and strain are shown in Fig. 5b. As the electrode interval decreases, the strain is increased. It can be seen from Fig. 5b that there is an optimal electrode width when the corresponding strain per unit voltage is the largest. The optimum electrode width and electrode interval s are independent of the substrate thickness. The optimum electrode width can be obtained when w/t=0.7. With small electrode intervals, the position deviation has a large influence on the voltage. When the electrode width is large, the "dead zone" between the electrodes can be observed. This field is perpendicular to the actuating direction x. For a small electrode width, there is a corresponding weak field between the electrodes. As shown in Fig. 5c, the optimal electrode width is 140 μm, i.e., when the substrate thickness is stable at 200 μm, the electrode interval is 1 mm, and the electrode width varies between 25~400 μm, the "dead zone" and electric field strength reach a balance value when electrode width w is 140 μm, which further verifies the optimum ratio of w/t=0.7.

The vector diagrams in Fig.6 show the concentrated electric fields with the electrode boundary under different electrode widths. The field strength in the area in Fig.6 is increased with increasing the w/t ratio. At the same time, the electrode direction is not affected. The results show that the presence of an uneven field boundary at the electrode boundary can lead to cracks in the piezoelectric substrate and cause damage to the device. With decreasing the strain, the polymer layer can be used as the buffer zone of the field and the zone of influence of stress concentration. It can be seen from Fig. 6 that when the substrate thickness is constant, the "dead zone" between the electrodes is increased as the electrode width increases.

3.2 Influence of substrate thickness t on actuating performance of SAW-IDT

Based on the optimal electrode width, the influence of the substrate thickness t on the output voltage was studied. Fig. 7 shows the effect of substrate thickness on the substrate. As the thickness of the substrate decreases, the strain increases. When w/t=0.7 and the electrode interval s=1 mm, the electric field along the direction of center axis x of the substrate corresponds to the values of three substrates, as shown in

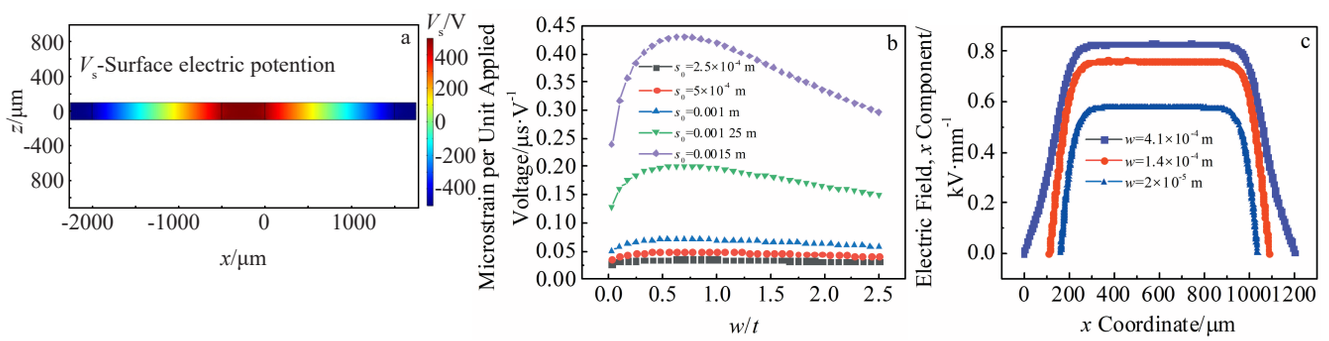

Fig.5 Influence of electrode width w or substrate thickness t on electric field: (a) IDT surface voltage; (b) strain response of IDT transducer (t= 200 μm, w/t=0.7); (c) electric field path diagram (t=200 μm, s=1 mm, V=50 V)

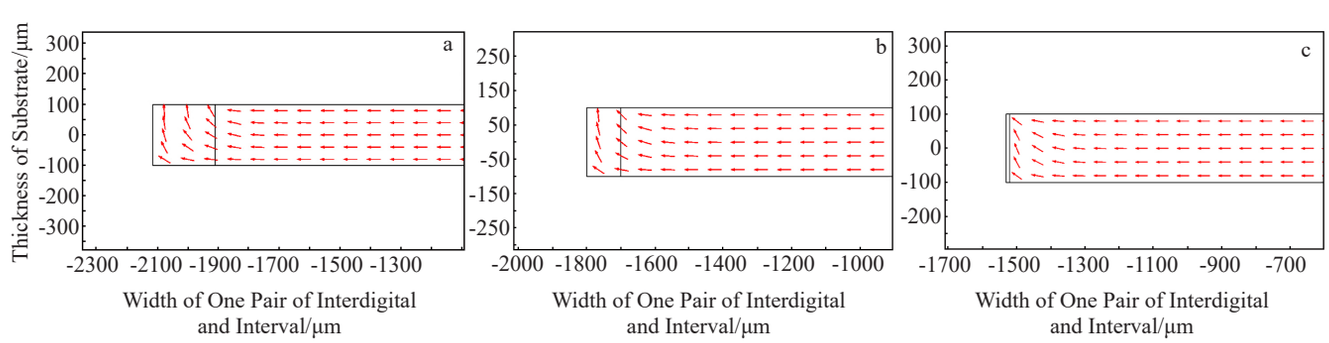

Fig.6 Electric field distributions with different electrode widths: (a) w=400 μm, (b) w=140 μm, and (c) w=25 μm

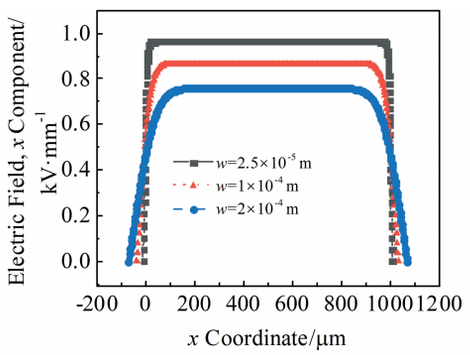

Fig.7 Effect of substrate on strain response

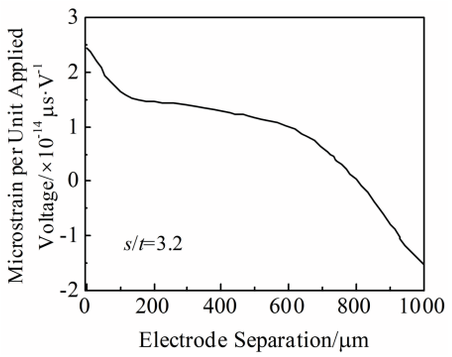

Fig.9 Relationship between microstrain and electrode separation

Fig. 8. As the substrate thickness decreases, the electric field possesses shorter distance along the in-plane direction, and the proportion of "dead zones" is decreased. With decreasing the substrate thickness, the electric field between the electrodes becomes larger, and the influence between the inverse electrodes becomes more direct. The results show that the width of the thin substrate and the electrode conform to the optimal ratio of w/t=0.7, which improves the actuating performance of SAW.

3.3 Effect of electrode interval *s* on actuating performance of SAW-IDT

To observe the effect of the electrode interval, the ratio of w/t was set as 0.7, and the electrode interval varied from 1 μm to 1000 μm. Eq. (3) shows the relationship between the electrode interval s and the strain S produced by the unit voltage:

$$\frac{S}{V}=\frac{d_{33}}{s} \tag{3}$$

where V is the applied voltage.

As shown in Fig. 9, the strain response of electrode interval changes with the electrode separation when the substrate thickness is 25 μm. As the electrode interval decreases, the microstrain per unit voltage increases. The small electrode interval can improve the actuating performance. When s=80 μm, the unit voltage increases sharply. According to the calculating result, when s/t>3.2, the greatest microstrain can be obtained.

4 Frequency Response of Prepared SAW-IDT

In this research, the screen-printing method[8] was used to prepare the interdigital electrode. The screen frame was processed and manufactured. The screen-printing plate was made of the photosensitive material and then used through the photolithography method. According to the finite element simulation analysis results of SAW-IDT optimization size, the key geometric dimensions of the electrode are shown in Table 2.

The prepared SAW-IDT electrode is shown in Fig. 10. The electrode prepared by screen-printing method is smooth and uniform with high precision and shows excellent electrical conductivity.

The Agilent5290 impedance analyzer uses the built-in frequency generator to generate a specific frequency for exciting the SAW-IDT. The response signal obtained from the measured SAW-IDT was sampled by the analog-to-digital

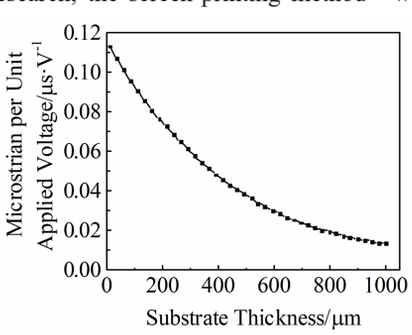

Fig. 8 Electric field caused by thickness change of three electrodes (w/t=0.7, s=1 mm, V=0.5 kV)

Table 2 Key dimensions of interdigital electrodes

Key dimension	Value
Electrode width, w/mm	0.25
Electrode interval, s/mm	0.25
Thickness of PZT basement, t/mm	0.7
Working area width, L/mm	14
Number of fingers on unilateral electrode	12

Fig.10 Appearance of SAW-IDT electrode

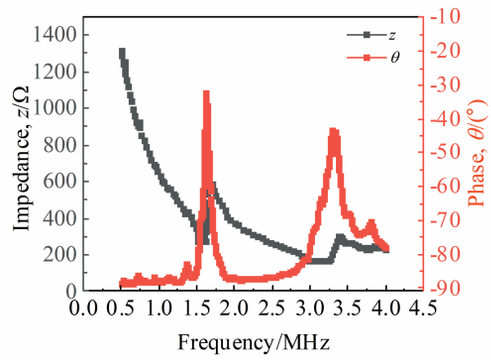

Fig.11 SAW-IDT impedance z and phase θ vs frequency

converter (ADC), and the discrete Fourier transform was performed through the digital signal processing (DSP). Fig.11 shows the relationship diagram of SAW-IDT impedance z and phase θ with frequency based on the continuous measurement of the real part value R and imaginary part value I of a frequency band. The first-order center frequency of the prepared SAW-IDT is 1.62 MHz. SAW-IDT in different frequency ranges can be obtained by adjusting the electrode interval, which can be used for detection components with different frequencies.

5 Conclusions

1) With different electrode intervals s and variation of the ratio of electrode width w to substrate thickness t, the optimal strain response can be obtained when w/t=0.7.

2) When s/t>3.2, the maximum strain can be obtained.

3) According to the optimization relation of the dimension parameters, the surface acoustic wave interdigital transducer (SAW-IDT) was prepared and the frequency response was tested by experiment, which provides a theoretical guide for the optimal design of SAW-IDT and structural health monitoring application.

References

1 Nguyen V H, Kaulen C, Simon U *et al*. *Sensor*[J], 2017, 17(12): 2931

2 Malocha D C. *IEEE Ultrasonics Symposium*[C]. Montreal: IEEE Press, 2004, 1: 302

3 Takpara R, Duquennoy M, Courtois C *et al*. *AIP Conference Proceedings*[C]. New York: AIP Publishing, 2016, 1706(1): 70 003

4 Yan X, Zhu R, Huang G L *et al*. *Health Monitoring of Structural and Biological Systems 2013*[C]. Bellingham: International Society for Optics and Photonics, 2013, 8695: 86 952

5 Zhou Q, Lam K H, Zheng H *et al*. *Progress in Materials Science* [J], 2014, 66: 87

6 Wang T X, Xie L Q, Xing J C *et al*. *Integrated Ferroelectrics*[J], 2017, 183(1): 8

7 Wang Z P, Luo Y, Zhao G Q *et al*. *Research in Nondestructive Evaluation*[J], 2016, 27(4): 204

8 Wang Z P, Jiang Z X, Chen L B *et al*. *AIP Advances*[J], 2018, 8(5): 55 303

9 Hashimoto K Y. *Surface Acoustic Wave Devices in Telecommunications*[M]. Berlin: Springer-Verlag, 2000

10 Mańka M, Rosiek M, Martowicz A *et al*. *11th IMEKO TC 10-Workshop on Smart Diagnostics of Structures*[C]. Kraków: Instrument Society of America, 2010

11 Mańka M. *Diagnostyka*[J], 2018, 19(1): 49

12 Wei M, Hrner A L, Zallo E *et al*. *Phys Rev Applied*[J], 2017, 9(1): 14 004

13 Jin J, Quek S T, Wang Q. *Ultrasonics*[J], 2005, 43(6): 481

14 Monkhouse R S C, Wilcox P W, Lowe M J S *et al*. *Smart Materials & Structures*[J], 2000, 9(3): 304

15 Hayward G, Hailu B, Farlow R *et al*. *Smart Structures & Materials 2001: Smart Structures & Integrated Systems*[C]. Singapore: International Society for Optics and Photonics, 2001

16 Ren B, Lissenden C J. *AIP Conference Proceedings*[J], 2016, 1706(1): 30 011

17 Bellan F, Bulletti A, Capineri L *et al*. *Sensors and Actuators A* [J], 2005, 123: 379

18 Wang Z P, Qian L, Fei Y *et al*. *Rare Metal Materials and Engineering*[J], 2020, 49(11): 3790

19 Lin C M, Chen Y Y, Wu T T. *Journal of Physics D: Applied Physics*[J], 2006, 39(3): 466

20 Stepinski T, Mańka M, Martowicz A *et al*. *SPIE Smart Structures & Materials+Nondestructive Evaluation & Health Monitoring*[C]. Las Vegas: SPIE, 2016, 9803: 98030N

21 Baravelli E, Senesi M, Ruzzene M *et al*. *IEEE Transactions on Instrumentation & Measurement*[J], 2013, 62(8): 2197

22 Tagawa K, Tokunaga K, Haneda H *et al*. *IEEE 2002-28th Annual Conference of the Industrial Electronics Society*[C]. Seville: IEEE Press, 2002(3): 2572

23 Weigel R, Kalabic F, Ostermayer G *et al*. *IEEE Transactions on Microwave Theory & Techniques* [J], 1997, 45(12): 2486

24 Mishra D, Singh A, Hussain D M A *et al*. *2016 3rd International Conference on Computing for Sustainable Global Development* [C]. New Delhi: IEEE Press, 2016

25 Nakamura K, Hirota K. *IEEE Transactions on Ultrasonics Ferroelectrics & Frequency Control*[J], 1996, 43(3): 467

26 Kuznetsova I, Nedospasov I, Smirnov A *et al*. *Ultrasonics*[J], 2019, 99: 105 961

27 He J, Leser P E, Leser W P *et al*. *Struct Health Monit*[J], 2018, 17(6): 1365

28 Sang S, Sandgren E, Wang Z. *Journal of the Acoustical Society of America*[J], 2017, 142(4): 2578

29 Holland R. *IEEE Transactions on Sonics and Ultrasonics*[J], 1968, 15(2): 97

单层声表面波叉指换能器(SAW-IDT)结构优化设计

王自平[1,2]，费　跃[1]，钱　磊[1]，薛　显[1]，Karthik　Reddy[2]
(1. 江苏大学 土木工程与力学学院 高端装备关键结构健康管理国际联合研究中心，江苏 镇江 212013)
(2. 北卡罗莱纳州立大学 机械与航空航天工程系，美国 罗利 27606)

摘　要：为优化单层声表面波换能器的驱动性能，改善现有δ函数分析方法在计算过程中的不足之处，采用有限元仿真优化方法对叉指式换能器的静力学性能进行了分析，研究了支路电极宽度w、电极间距s和基片厚度t对驱动性能的影响。仿真结果表明，当w/t=0.7时，可以得到最佳应变响应；当s/t＞3.2时，可以得到最大应变。同时还得出了电极间距越小，驱动电压越低的结论。根据仿真优化结果制备了声表面波叉指换能器（SAW-IDT），并进行了频率响应测试。研究结果为声表面波叉指换能器的制备、性能测试和应用提供了指导。

关键词：叉指换能器；结构优化设计；驱动性能

作者简介：王自平，男，1979年生，博士，副教授，江苏大学土木工程与力学学院，江苏 镇江 212013，E-mail：wzpxx2004@126.com